IEEE Access
Multidisciplinary | Rapid Review | Open Access Journal

Received 19 September 2022, accepted 19 October 2022, date of publication 28 November 2022,
date of current version 1 December 2022.

Digital Object Identifier 10.1109/ACCESS.2022.3225095

RESEARCH ARTICLE

A Rotor Position Signal-Free Based Field Current Estimation Method for Brushless Synchronous Starter/Generator

ZAN ZHANG, WEIZHOU LI, LUHUAN SHI, JUNLEI MA, AND ZHIFENG YIN
School of Electrical and Mechanical Engineering (Engineering Training Center), Xuchang University, Xuchang 461000, China

Corresponding author: Zhifeng Yin (zz@xcu.edu.cn)

This work was supported in part by the Scientific and Technological Key Project in Henan Province under Grant 202102210307, and in part by the Key Scientific Research Projects of Colleges and Universities in Henan Province under Grant 19A470007 and Grant 21B470008.

ABSTRACT This article proposed a position signal-free field current estimation method for brushless synchronous starter/generator (BSSG). Generally, the estimation of the field current of BSSG depends on the position signals provided by a physical sensor or position estimation algorithm. However, there are risks in using the traditional method when the position sensor is broken or using estimated position information to evaluate the field current. To overcome this problem, this paper proposes a position signal-free estimation method. In this method, the mathematical relationship between the field current of the main machine (MM) and the current vector modulus (CVM) of the main exciter (ME) rotor currents are analyzed. The theoretical findings reveal that the field current of the main machine (MM) equates to the minimum or $\sqrt{3}/2$ times maximum distance during the rotating trajectory of ME's rotor CVM in both rotating and stationary coordinates. Since the ME's rotor CVM is independent of the rotor position information, the estimation of the field current of BSSG can be achieved without the rotor position signal departing in. Finally, an experiment platform is established to emulate the BSSG, and experimental results validate the theoretical findings.

INDEX TERMS Field current, estimation, position signal-free, rotor current vector modulus, BSSG.

I. INTRODUCTION

With the development of full/more electric airplanes, the integrated starter/generator (ISG) has become the trend of future power systems due to its small volume, lower weight, and fuel-saving characteristics [1], [2], [3], [4]. Among various topologies of ISG, the brushless synchronous starter/generator (BSSG) has attracted widespread attention for its high reliability, lower maintenance costs [5].

Generally, the BSSG consisted of three coaxially mounted machines (as shown in Fig.1): a main synchronous machine (MM), a main exciter (ME), and a pre-exciter (PE) [6]. To start engine, the ME stator windings should be powered by a three-phase source first. Secondly, the generated three-phase electric power of ME rotor windings is rectified to DC field current for MM field winding by a rotating rectifier. And then, the MM obtains the ability to start an aircraft engine. With a property field current value and MM control algorithm, the MM could be operated as an engine starter [7]. However, due to the brushless structure of the excitation system, the field current cannot be measured directly for closed-loop control. It desperately needs to be estimated.

To estimate the field current, [8] presents a ME rotor current/voltage-based method, and reference [9] presents an average-value model of the rotating rectifier to estimate the MM's field current. Although these methods have high precision, the estimation process requires rotor position information.

There are two commonly used ways to obtain the rotor position information to get a rotor position. The most accurate method is using a position sensor to obtain position information, but the position sensor is prone to interference or malfunction. The second method is the most popular way to estimate position using a sensorless algorithm. The

The associate editor coordinating the review of this manuscript and approving it for publication was Zhuang Xu.

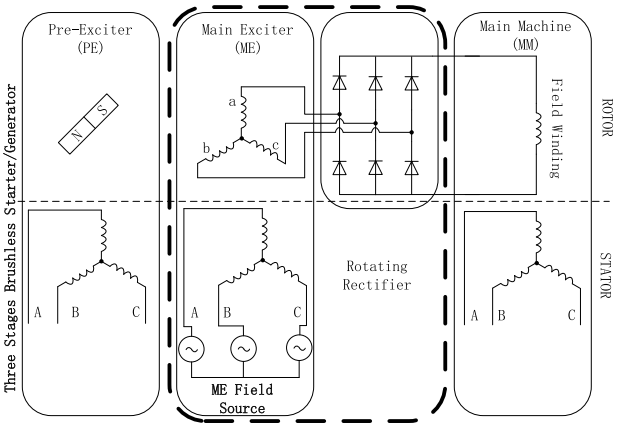

FIGURE 1. Three phase bridge rotating rectifier.

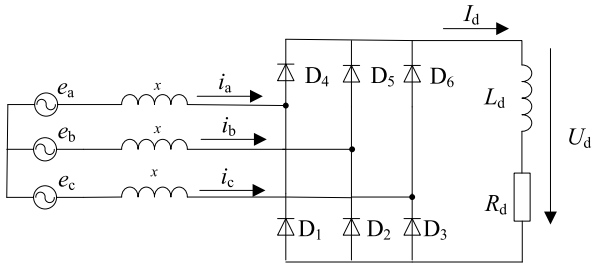

FIGURE 2. Three phase bridge rotating rectifier.

senseorless algorithms are widely used in permanent magnet motors at stationery and rotation conditions. In the stationary and low-speed region, the high frequency (HF) signal injection method is more precise than the back electromotive force (BEMF) based approach. However, during the high-speed region, the BEMF-based process is precise enough to replace the HF signal injection method and reduce the iron loss, torque, and noise.

For the BSSG, during the starting process, the highly saturated wound rotor iron-core severely changes the saliency of the MM. Meanwhile, the existence of damping windings makes the HF signal injection method even hard to obtain a natural rotor position. Therefore, many researchers have conducted in-depth research on position estimation methods to get an exact rotor position. Reference [10] injects an HF signal voltage into the d-axis and extracts the rotor position signal at MM stator windings. Reference [11] using the 6th sequence harmonic voltage determined by the rotating rectifier and the HF voltage signal injected into the field-winding of MM. It extracts the rotor position signal from MM's stator windings. Reference [12] injects a high-frequency signal into the ME's stator. A response of high-frequency signals with the rotor information is indirectly coupled to the field windings of the MM. Then, the envelope demodulation method for the rotor position estimation with the unitized filter design of bandpass filter, low-phase filter, and second-order generated integrator is employed to estimate a rotor position. Reference [13] injects high-frequency signals into the ME and uses a second-order generalized integrator-based frequency-insensitive demodulation method to calculate rotor position. Reference [14] injects two HF pulsating voltages with different frequencies into phase alpha and phase beta of MM stator windings. It then estimates the rotor position from ME's stator windings and compensates the position signal by a first quadrant definite integral method. Reference [15] presents a rotor position estimation method based on the harmonic currents in ME stator windings without HF signal injection. It extracts the rotor position information from the ME stator currents. Reference [16] and [17] injects an HF voltage into MM stator windings and extracts the rotor position signal at ME stator windings. Reference [18] and [19] extracts the rotor position from the hexagonal trajectory of the rotor current space vector of ME to avoid any HF signal analysis.

Although the sensorless position algorithm dramatically improves the reliability of the starter/generator integrated system. However, using an estimated position signal to evaluate the field current of the MM further, the system's reliability is difficult to guarantee. This paper proposes a rotor position signal-free field current estimation method to address this problem, which can extract the field current from the ME rotor current modulus independent of the rotor position signal.

This article is organized as follows. In section II, the rotating rectifier and the excitation system modeling are established, and the relationship among the field current of MM, the ME rotor current vector module, the ME stator currents, and voltages is analyzed. In section III, the ME rotor CVM-based field current estimation strategy is comprehension clarified. The experimental results are analyzed in section IV, and section V is the conclusion section.

II. SYSTEM MODELING

Before modeling, some assumptions are made to reduce the difficulty and complexity of analyzing: (i) both exciter stator and rotor windings are star-connected; (ii) the induced fundamental back EMF of exciter rotor windings are three-phase balanced sine wave; (iii) the saturation phenomenon of iron core and coil-damping effects are neglected; (iv) the ME rotor winding resistances are neglected.

A. ROTATING RECTIFIER

The equivalent three-phase rotating rectifier circuit is shown in Figure 2.

In Fig.2, e_a, e_b, e_c, i_a, i_b and i_c represent the fundamental back EMF and current of ME three-phase rotor windings, respectively. I_d, U_d represent the rectified field current and voltage of MM. x represent the ME rotor leakage inductance. L_d and R_d represent the equivalent inductance and resistance of MM field winding. D_1, D_2, D_3, D_4, D_5 and D_6 represent the six rotating diodes. In a back EMF period, the TBAES three-phase rotor current expresses are shown as

below [20], [21]:

$$I_a = \begin{cases} I_f;\ wt \in \left(\theta - \frac{\pi}{3}, \frac{\pi}{3}\right) \\ \frac{\cos\left(wt - \frac{\pi}{3}\right) - \cos\theta}{1 - \cos\theta} I_f;\ wt \in \left(\frac{\pi}{3}, \frac{\pi}{3} + \theta\right) \\ 0;\ wt \in \left(\frac{\pi}{3} + \theta, \frac{2\pi}{3}\right) \\ \frac{\cos\left(wt - \frac{2\pi}{3}\right) - 1}{1 - \cos\theta} I_f;\ wt \in \left(\frac{2\pi}{3}, \frac{2\pi}{3} + \theta\right) \\ -I_f;\ wt \in \left(\frac{2\pi}{3} + \theta, \frac{4\pi}{3}\right) \\ \frac{\cos\theta - \cos\left(wt - \frac{4\pi}{3}\right)}{1 - \cos\theta} I_f;\ wt \in \left(\frac{4\pi}{3}, \frac{4\pi}{3} + \theta\right) \\ 0;\ wt \in \left(\frac{4\pi}{3} + \theta, \frac{5\pi}{3}\right) \\ \frac{1 - \cos\left(wt - \frac{5\pi}{3}\right)}{1 - \cos\theta} I_f;\ wt \in \left(\frac{5\pi}{3}, \frac{5\pi}{3} + \theta\right) \end{cases} \tag{1}$$

$$I_b = \begin{cases} \frac{\cos\theta - \cos wt}{1 - \cos\theta} I_f;\ wt \in (0, \theta) \\ 0;\ wt \in \left(\theta, \frac{\pi}{3}\right) \\ \frac{1 - \cos\left(wt - \frac{\pi}{3}\right)}{1 - \cos\theta} I_f;\ wt \in \left(\frac{\pi}{3}, \frac{\pi}{3} + \theta\right) \\ I_f;\ wt \in \left(\frac{\pi}{3} + \theta, \pi\right) \\ \frac{\cos\left(wt - \pi\right) - \cos\theta}{1 - \cos\theta} I_f;\ wt \in (\pi, \pi + \theta) \\ 0;\ wt \in \left(\pi + \theta, \frac{4\pi}{3}\right) \\ \frac{\cos\left(wt - \frac{4\pi}{3}\right) - 1}{1 - \cos\theta} I_f;\ wt \in \left(\frac{4\pi}{3}, \frac{4\pi}{3} + \theta\right) \\ -I_f;\ wt \in \left(\frac{4\pi}{3} + \theta, 2\pi\right) \end{cases} \tag{2}$$

$$I_c = \begin{cases} \frac{\cos wt - 1}{1 - \cos\theta} I_f;\ wt \in (0, \theta) \\ -I_f;\ t \in \left(\theta, \frac{2\pi}{3}\right) \\ \frac{\cos\theta - \cos\left(wt - \frac{2\pi}{3}\right)}{1 - \cos\theta} I_f;\ wt \in \left(\frac{2\pi}{3}, \frac{2\pi}{3} + \theta\right) \\ 0;\ wt \in \left(\frac{2\pi}{3} + \theta, \pi\right) \\ \frac{1 - \cos\left(wt - \pi\right)}{1 - \cos\theta} I_f;\ wt \in (\pi, \pi + \theta) \\ I_f;\ wt \in \left(\pi + \theta, \frac{5\pi}{3}\right) \\ \frac{\cos\left(wt - \frac{5\pi}{3}\right) - cos\theta}{1 - \cos\theta} I_f;\ wt \in \left(\frac{5\pi}{3}, \frac{5\pi}{3} + \theta\right) \\ 0;\ wt \in \left(\frac{5\pi}{3} + \theta, 2\pi\right) \end{cases} \tag{3}$$

The alpha and beta-axis rotor currents in the rotor coordinate system are expressed as below:

$$\begin{cases} i_\alpha = i_a \\ i_\beta = \frac{\sqrt{3}}{3}(i_b - i_c) \end{cases} \tag{4}$$

Normally, the ME's rotor current vector module can be as equivalent (4):

$$|i_r| = \sqrt{i_\alpha^2 + i_\beta^2} \tag{5}$$

Then, the ME's rotor CVM can be obtained according to (1-5), as in (6), shown at the bottom of the next page.

Taking the extreme value of the current CVM, we get the maximum $|i_r|_{max}$ and minimum $|i_r|_{min}$ values as follow:

$$\begin{cases} |i_r|_{max} = \frac{2}{\sqrt{3}} \quad i_f \\ |i_r|_{min} = \qquad i_f \end{cases} \tag{7}$$

Equation (7) reveals that the MM field current value is related to the ME rotor current CVM. And, if the calculation of rotor current CVM is independent of the rotor position information, the position signal-less based field current estimation achieves.

B. THE EXCITATION SYSTEM

The flux linkage equation and voltage equation of ME stator and rotor windings in the α-axis and β-axis are shown as (8) and (9):

$$\begin{bmatrix} \psi_{s\alpha} \\ \psi_{s\beta} \\ \psi_{r\alpha} \\ \psi_{r\beta} \end{bmatrix} = \begin{bmatrix} L_s & 0 & M_m cos\eta & -M_m sin\eta \\ 0 & L_s & M_m sin\eta & M_m cos\eta \\ M_m cos\eta & M_m sin\eta & L_r & 0 \\ -M_m sin\eta & M_m cos\eta & 0 & L_r \end{bmatrix} \times \begin{bmatrix} i_{s\alpha} \\ i_{s\beta} \\ i_{r\alpha} \\ i_{r\beta} \end{bmatrix} \tag{8}$$

$$\begin{bmatrix} u_{s\alpha} \\ u_{s\beta} \\ u_{r\alpha} \\ u_{r\beta} \end{bmatrix} = \begin{bmatrix} R_s & 0 & 0 & 0 \\ 0 & R_s & 0 & 0 \\ 0 & 0 & R_r & 0 \\ 0 & 0 & 0 & R_r \end{bmatrix} \begin{bmatrix} i_{s\alpha} \\ i_{s\beta} \\ i_{r\alpha} \\ i_{r\beta} \end{bmatrix} + P\left(\begin{bmatrix} \psi_{s\alpha} \\ \psi_{s\beta} \\ \psi_{r\alpha} \\ \psi_{r\beta} \end{bmatrix}\right) \tag{9}$$

In equations (8) and (9), $\psi_{s\alpha}$, $\psi_{s\beta}$, $i_{s\alpha}$, $i_{s\beta}$, $u_{s\alpha}$, and $u_{s\beta}$ represent the ME's stator windings α and β-axis flux linkages, voltages, and currents, respectively. $\psi_{r\alpha}$, $\psi_{r\beta}$, $i_{r\alpha}$, $i_{r\beta}$, $u_{r\alpha}$ and $u_{r\beta}$ represent the ME's rotor windings α and β-axis flux linkages, voltages, and currents, respectively. R_s and R_r represent the ME's stator and winding phase resistances respectively. M_m represents mutual inductances between ME's stator and rotor windings. η represents the electric degree between the ME's stator A phase winding axis

and B phase winding axis. L_r represents the self-inductance of ME's stator and rotor phase windings.

Generally, there are two voltage and current sensors in the ME stator for collecting the phase voltage and current signals. Thus, $i_{s\alpha}$, $i_{s\beta}$, $u_{s\alpha}$, and $u_{s\beta}$ can be calculated by i_A, i_B, u_A, and u_B using a Clark transform:

$$\begin{bmatrix} i_{s\alpha} \\ i_{s\beta} \\ i_{so} \end{bmatrix} = \begin{bmatrix} \frac{2}{3} & -\frac{1}{3} & -\frac{1}{3} \\ 0 & \frac{\sqrt{3}}{3} & -\frac{\sqrt{3}}{3} \\ \frac{1}{3} & \frac{1}{3} & \frac{1}{3} \end{bmatrix} \begin{bmatrix} i_A \\ i_B \\ -i_A - i_B \end{bmatrix} \tag{10}$$

$$\begin{bmatrix} u_{s\alpha} \\ u_{s\beta} \\ u_{so} \end{bmatrix} = \begin{bmatrix} \frac{2}{3} & -\frac{1}{3} & -\frac{1}{3} \\ 0 & \frac{\sqrt{3}}{3} & -\frac{\sqrt{3}}{3} \\ \frac{1}{3} & \frac{1}{3} & \frac{1}{3} \end{bmatrix} \begin{bmatrix} u_A \\ u_B \\ -u_A - u_B \end{bmatrix} \tag{11}$$

To estimate ME's rotor CVM, the rotor α-axis and β-axis currents must be estimated first. Using equations (9), (10), and (11), we get

$$\begin{cases} \psi_{s\alpha} = \int (u_{s\alpha} - R_s i_{s\alpha})\, dt \\ \psi_{s\beta} = \int \left(u_{s\beta} - R_s i_{s\beta}\right) dt \end{cases} \tag{12}$$

Then, $i_{r\alpha}$ and $i_{r\beta}$ can be calculated as follows:

$$i_{ra} = \frac{\begin{vmatrix} \frac{\psi_{s\alpha} - L_s i_{s\alpha}}{M_m} & -sin\eta \\ \frac{\psi_{s\beta} - L_s i_{s\beta}}{M_m} & cos\eta \end{vmatrix}}{\begin{vmatrix} cos\eta & -sin\eta \\ sin\eta & cos\eta \end{vmatrix}} \tag{13}$$

$$\begin{cases} \frac{2}{\sqrt{3}} I_f \sqrt{\frac{1 + cos^2 wt - \cos\theta + cos^2\theta - \cos wt\,(1 + \cos\theta)}{(-1 - \cos\theta)^2}} \\ , wt \in (0, \theta) \\ \frac{2}{\sqrt{3}} I_f, wt \in \left(\theta, \frac{\pi}{3}\right) \\ \frac{2}{\sqrt{3}} I_f \sqrt{\frac{1 + cos^2\left(wt - \frac{\pi}{3}\right) - \cos\theta + cos^2\theta - \cos wt\,(1 + \cos\theta)}{(-1 - \cos\theta)^2}} \\ , wt \in \left(\frac{\pi}{3}, \frac{\pi}{3} + \theta\right) \\ \frac{2}{\sqrt{3}} I_f, wt \in \left(\frac{\pi}{3} + \theta, \frac{2\pi}{3}\right) \\ \frac{2}{\sqrt{3}} I_f \sqrt{\frac{1 + cos^2\left(wt - \frac{2\pi}{3}\right) - \cos\theta + cos^2\theta - \cos wt\,(1 + \cos\theta)}{(-1 - \cos\theta)^2}} \\ , wt \in \left(\frac{2\pi}{3}, \frac{2\pi}{3} + \theta\right) \\ \frac{2}{\sqrt{3}} I_f, wt \in \left(\frac{\pi}{3} + \theta, \pi\right) \\ \frac{2}{\sqrt{3}} I_f \sqrt{\frac{1 + cos^2\left(wt - \pi\right) - \cos\theta + cos^2\theta - \cos wt\,(1 + \cos\theta)}{(-1 - \cos\theta)^2}} \\ , wt \in (\pi, \pi + \theta) \\ \frac{2}{\sqrt{3}} I_f, wt \in \left(\pi + \theta, \frac{4\pi}{3}\right) \\ \frac{2}{\sqrt{3}} I_f \sqrt{\frac{1 + cos^2\left(wt - \frac{4\pi}{3}\right) - \cos\theta + cos^2\theta - \cos wt\,(1 + \cos\theta)}{(-1 - \cos\theta)^2}} \\ , wt \in \left(\frac{4\pi}{3}, \frac{4\pi}{3} + \theta\right) \\ \frac{2}{\sqrt{3}} I_f, wt \in \left(\frac{4\pi}{3} + \theta, \frac{5\pi}{3}\right) \\ \frac{2}{\sqrt{3}} I_f \sqrt{\frac{1 + cos^2\left(wt - \frac{5\pi}{3}\right) - \cos\theta + cos^2\theta - \cos wt\,(1 + \cos\theta)}{(-1 - \cos\theta)^2}} \\ , wt \in \left(\frac{5\pi}{3}, \frac{5\pi}{3} + \theta\right) \\ \frac{2}{\sqrt{3}} I_f, wt \in \left(\frac{5\pi}{3} + \theta, 2\pi\right) \end{cases} \tag{6}$$

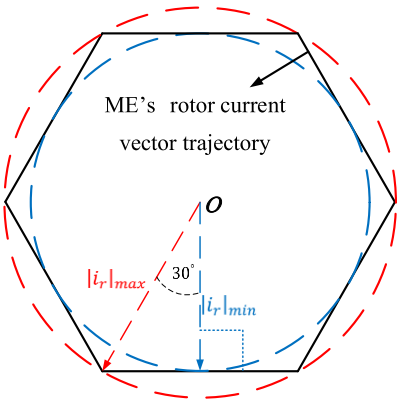

FIGURE 3. ME's rotor current vector trajectory.

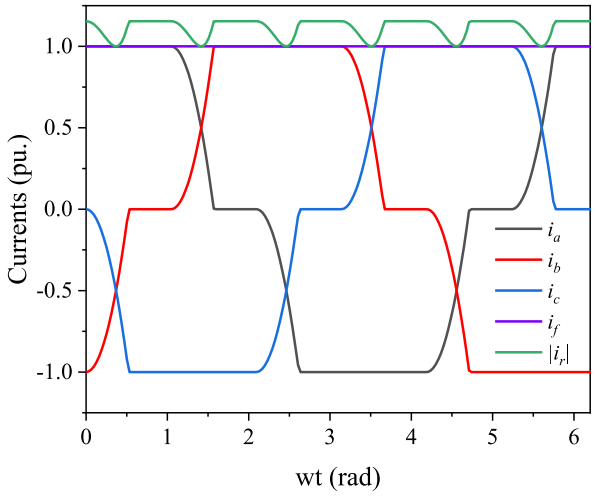

FIGURE 4. ME's rotor current vector Module and three-phase currents.

$$i_{r\beta} = \frac{\begin{vmatrix} cos\eta & \frac{\psi_{s\alpha} - L_s i_{s\alpha}}{M_m} \\ sin\eta & \frac{\psi_{s\beta} - L_s i_{s\beta}}{M_m} \end{vmatrix}}{\begin{vmatrix} cos\eta & -sin\eta \\ sin\eta & cos\eta \end{vmatrix}} \tag{14}$$

Finally, the ME's rotor CVM can be calculated as follows:

$$\begin{aligned} |i_r| &= \sqrt{i_{ra}^2 + i_{rb}^2} \\ &= \sqrt{\frac{2}{M_m^2}\left[\psi_{s\alpha}^2 + \psi_{s\beta}^2 - 2\left(\psi_{s\alpha} L_s i_{s\alpha} + \psi_{s\beta} L_s i_{s\beta}\right)\right]} \end{aligned} \tag{15}$$

The formula (15) presents that $|i_r|$ is only a function of $\psi_{s\alpha}$, $\psi_{s\beta}$, $i_{s\alpha}$ and $i_{s\beta}$. Since parameters $\psi_{s\alpha}$, $\psi_{s\beta}$, $i_{s\alpha}$ and $i_{s\beta}$ are independent of the rotor position η. Therefore, $|i_r|$ is also not a function of rotor position η.

III. ROTOR POSITION SIGNAL FREE MM FIELD CURRENT ESTIMATION STRATEGY

A. MM FIELD CURRENT ESTIMATION METHOD

Through the previous analysis, we get the following conclusions:

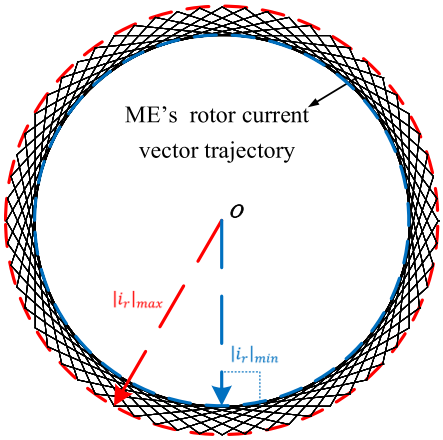

FIGURE 5. ME's rotor current vector trajectory (in stationary coordinate).

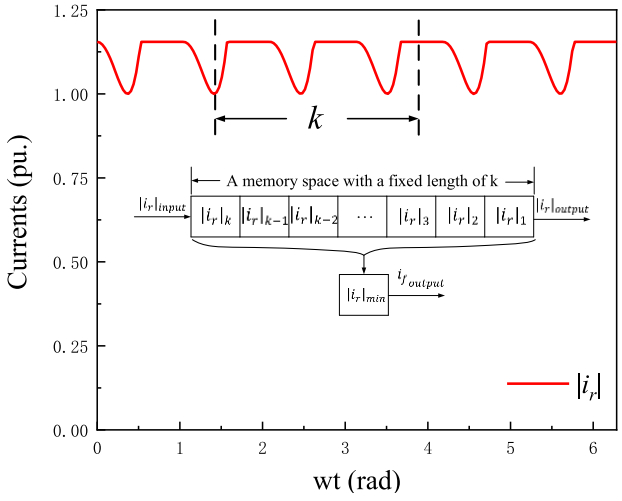

FIGURE 6. Moving minimum algorithm.

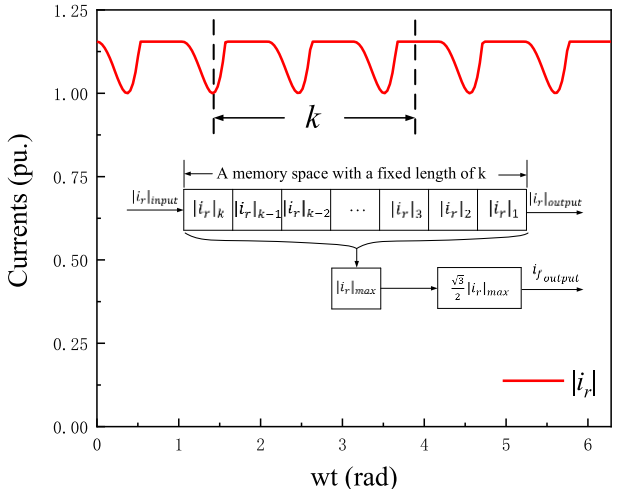

FIGURE 7. Moving maximum algorithm.

1) The MM's field current i_f equates to the minimum or $\sqrt{3}/2$ times of maximum of ME's rotor current CVM.

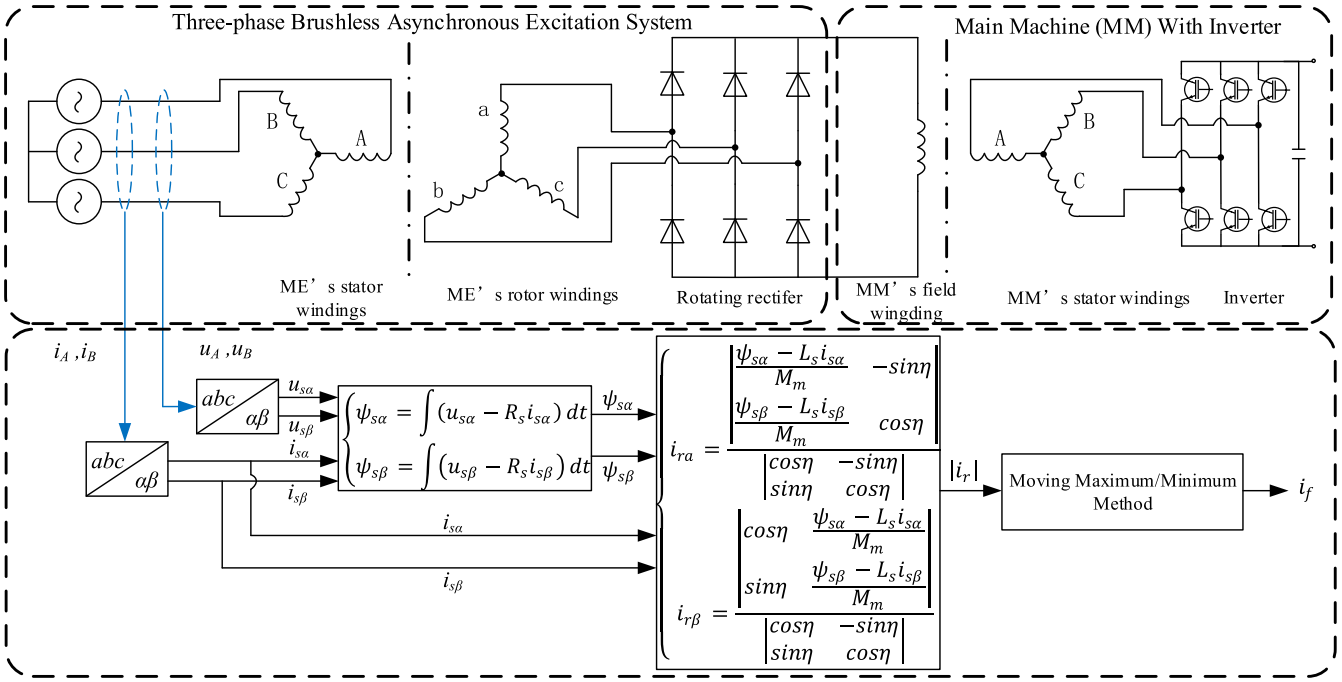

FIGURE 8. Schematic of the position signal free MM's field current estimation procedure.

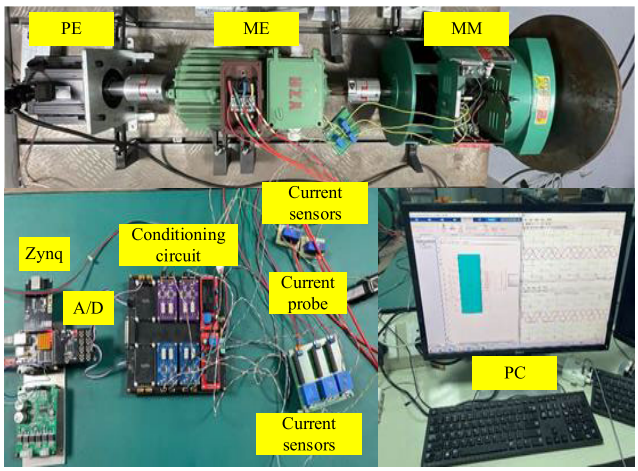

FIGURE 9. Real-time Rapid Prototyping Experimental platform based on Linux-Matlab/Simulink.

2) $|i_r|$ can be calculated by using ME's stator winding voltage and current.

Fig.3 shows that the current vector locus is a regular hexagon. Suppose the inscribed circle or circumscribed circle can be obtained in real-time by using the geometric characteristics of the regular hexagon and combined with the above conclusion 1. In that case, the excitation current of the main generator can be obtained practically. However, suppose the current vector trace of the exciter rotor is observed from the exciter stator side. In that case, the current vector trace is obtained as a rotating hexagon (shown in Fig.4). Finding a rotated hexagon's circular or circumscribed circle is a relatively complicated process.

To avoid complex geometric analysis, this paper uses the moving extreme value method to directly obtain the MM excitation current.

The moving extremum method opens a fixed-length first-in-first-out (FIFO) space in the memory. Every time the data is updated in the memory, the processor finds the minimum/maximum value in FIFO and uses this value further to solve the field current of the main generator.

It can be seen from conclusion one that there are two methods to obtain the MM field current. For the minimum ME rotor CVM method, the schematic diagram is shown in Figure 5. Every time, the processor pushes a new $|i_r|_k$ into the FIFO and pops an old $|i_r|_1$ out of the FIFO. Meanwhile, the processor finds the minimum $|i_r|_{min}$ in FIFO and uses the minimum $|i_r|_{min}$ as the MM field current $\left|i_f\right|$.

The same as moving minimum algorithms, the moving maximum algorithm (shown in figure 6) finds out the maximum $|i_r|_{max}$ in FIFO and uses $\sqrt{3}/2$ times $|i_r|_{max}$ as the MM field current $\left|i_f\right|$.

As seen from the schematic diagrams of the algorithms shown in Figures 5 and 6, the length 'k' of the FIFO is a crucial variable for the extremum extraction algorithm. Since the ME's rotor CVM is a periodic function, each period has one maximum value and one minimum value. If the FIFO stores multiple ME's rotor CVM periods, the obtained maximum/minimum value are the extreme values of numerous periods, and the final MM field current delay is significant. Conversely, if the FIFO storage space is small, typically less

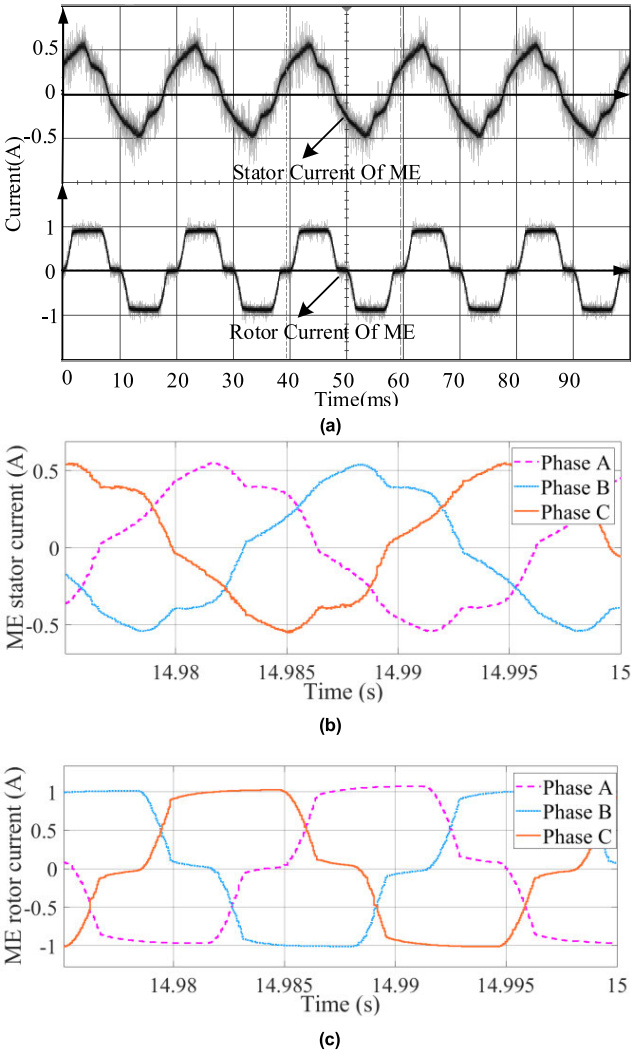

FIGURE 10. Stator and rotor current of ME at 50Hz fundamental frequency. (a) Stator and rotor current of ME measured by oscilloscope. (b) The stator three-phase current of ME measured on the experimental set. (c) The rotor three-phase current of ME measured on the experimental set.

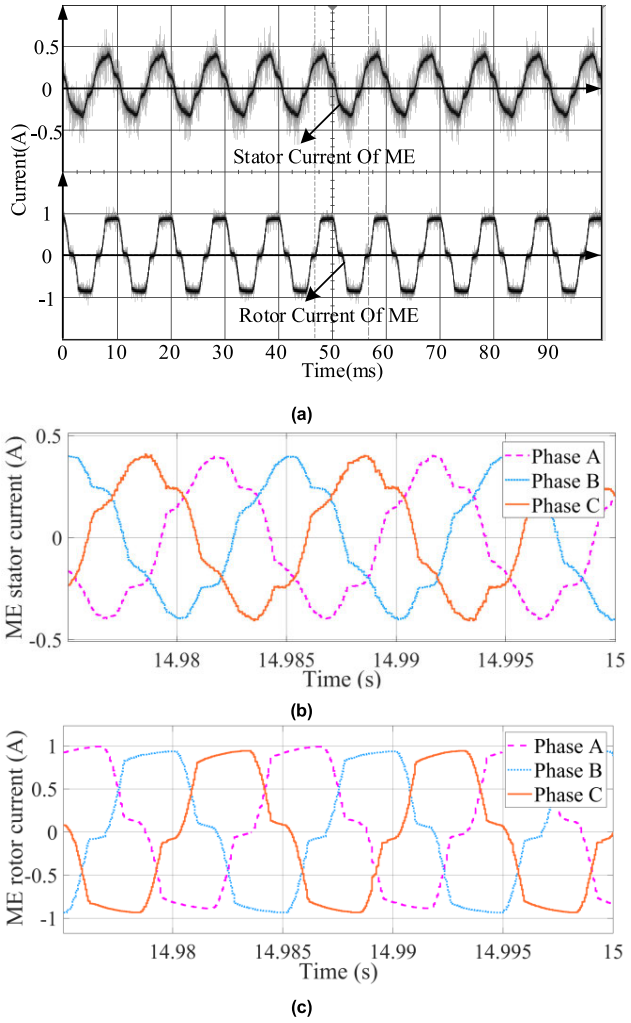

FIGURE 11. Stator and rotor current of ME at 100Hz fundamental frequency. (a) Stator and rotor current of ME measured by oscilloscope. (b) The stator three-phase current of ME measured on the experimental set. (c) The rotor three-phase current of ME measured on the experimental set.

than one power period, then the extremes in the FIFO are not true of ME's rotor CVM extremes. Therefore, the FIFO space needs to be able to store about two periods (minimum period) of data. Too short or too long is not conducive to extracting the field current of the MM.

B. MM FIELD CURRENT ESTIMATION STRATEGY

The schematic of the MM field current estimation strategy is illustrated in Fig.7. At the beginning of the algorithm, the voltage and current sensors on the stator side of ME send the collected voltage and current signals to the controller, firstly. Then, the controller performs filtering processing on the voltage and current signals and simultaneously opens up a section of FIFO storage space in the memory. Next, the controller obtains the modulo value of the exciter rotor current vector according to formula 10-15 and uses the moving average method to get the extreme value in the FIFO sequence. Finally, the extreme value is further processed and output as the excitation current i_f of the MM.

IV. EXPERIMENTAL EVALUATION

A. EXPERIMENTAL SETUP

A real-time rapid prototyping experimental platform based on Linux-MATLAB/Simulink is established to verify the proposed field current estimation method, as shown in figure 9. In the platform, the ME is emulated by an industry wound rotor induction motor, a brushed wound rotor synchronous generator as the MM, and a three-phase rectifier playing as a rotating rectifier. The parameters of ME and MM are shown in tables 1 and 2. The primary control unit adopts Xilinx Zynq 7020 (ARM+FPGA) in the experimental platform. The analog-to-digital conversion unit adopts A/D 7606, using voltage sensor module LEMLV25-P to

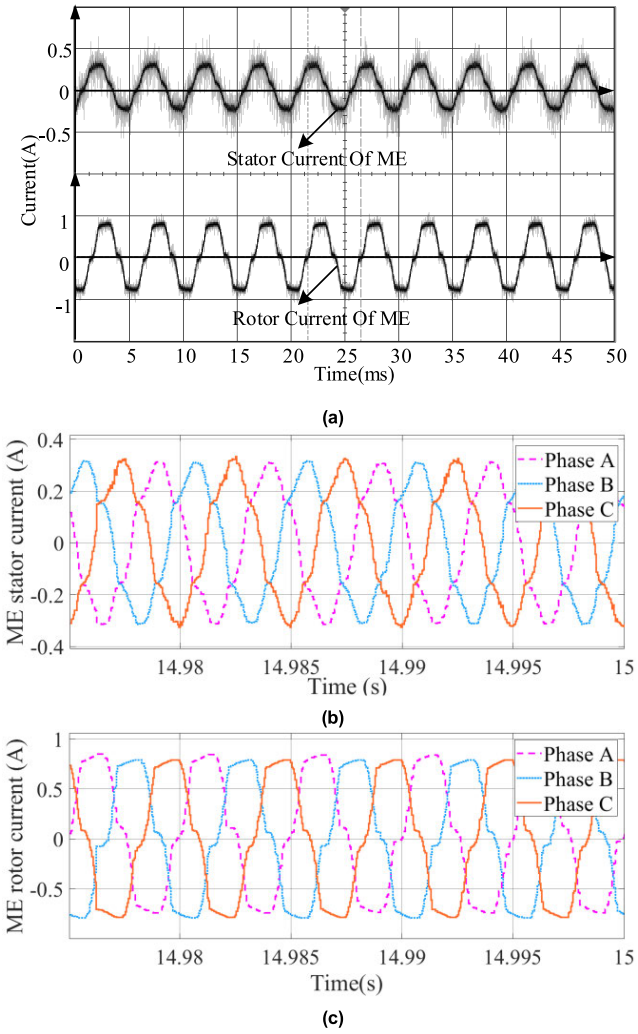

FIGURE 12. Stator and rotor current of ME at 200Hz fundamental frequency. (a) Stator and rotor current of ME measured by oscilloscope. (b) The stator three-phase current of ME measured on the experimental set. (c) The rotor three-phase current of ME measured on the experimental set.

collect the stator voltages of the exciter, using current sensor module LEM100-P to collect the stator and rotor currents of the exciter. The host computer communicates with the Zynq system in real-time through Gigabit Ethernet in Simulink. The computation steps running in the ARM is 0.00005 seconds (20k).

In this paper, the stator three-phase voltage and current and the rotor three-phase current of ME in the system are measured by an experimental set. Then the vector modulus of ME rotor current and the field current value of MM can be calculated by the measured value of voltage and current on the stator side of ME, which is called the estimated value in this paper. At the same time, the vector modulus of ME rotor current and the field current value of MM calculated by the measured value of rotor side current of ME is called the actual value in this paper. Finally, the accuracy of the proposed field current estimation method

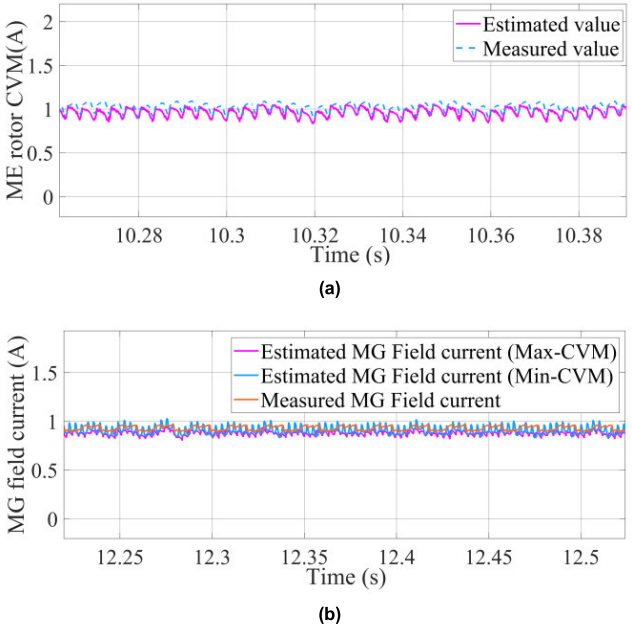

FIGURE 13. Waveform of ME rotor current and MM field current at fundamental frequency 50Hz. (a) ME rotor current Vector Modulus Waveform. (b) MM excitation current waveform.

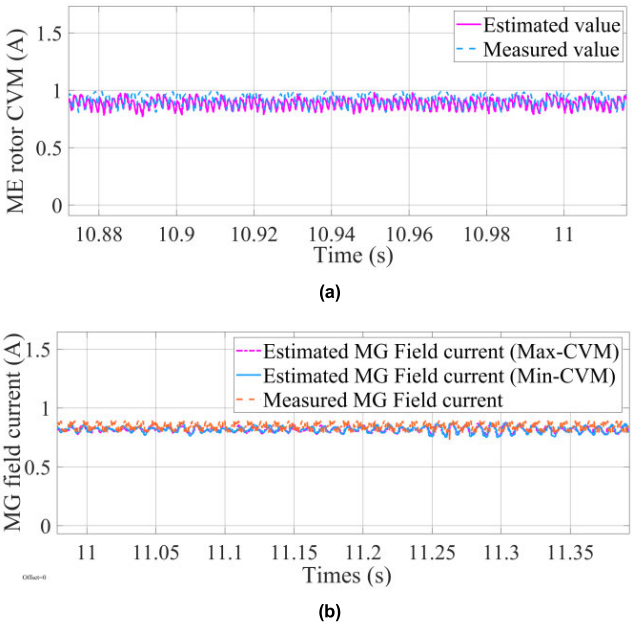

FIGURE 14. Waveform of ME rotor current and MM field current at fundamental frequency 100Hz. (a) ME rotor current Vector Modulus Waveform. (b) MM excitation current waveform.

is verified by comparing the estimated value with the real value.

B. ESTIMATION RESULT OF FIELD CURRENT WHEN MM IS STATIONARY

In the stationary condition, the excitation source of ME is setting the fundamental frequency to 50Hz, 100Hz, and 200Hz,

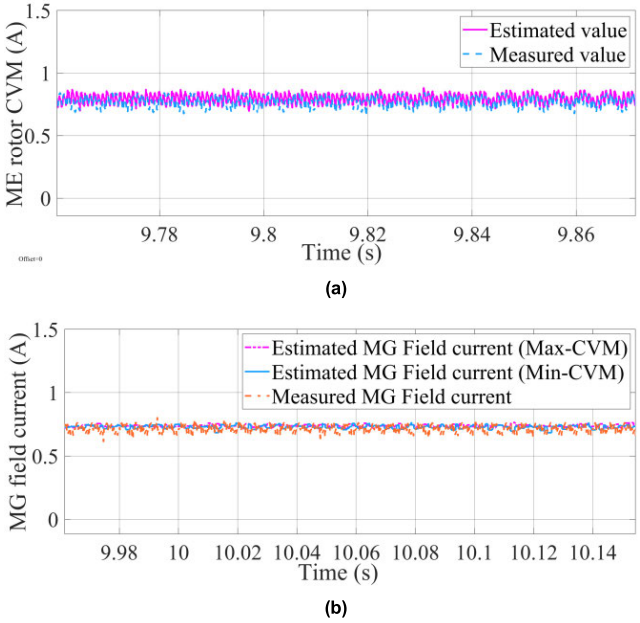

FIGURE 15. Waveform of ME rotor current and MM field current at fundamental frequency 200Hz. (a) ME rotor current Vector Modulus Waveform. (b) MM excitation current waveform.

TABLE 1. Parameters of the ME.

Symbol	Quantity	Value
n_p	Poles	6
P_N	Nominal power	1.6 kW
n_N	Nominal speed	845 r/min
V_n	Nominal voltage	380V Y
f_N	Nominal frequency	50 Hz
I_s	Nominal current (stator)	4.7 A
I_r	Nominal current (rotor)	11.2 A
R_s	Stator resistor	4.56 Ω
L_s	stator self-inductance	0.2813 H
M_m	mutual inductance	0.0523 H
R_r	Rotor resistor	0.45 Ω

TABLE 2. Parameters of the MM.

Symbol	Quantity	Value
n_{mp}	Poles	2
P_{mN}	Nominal power	15 kW
n_{mN}	Nominal speed	1500 r/min
V_{mn}	Nominal voltage	400V Y
fm_N	Nominal frequency	50 Hz
I_{ms}	Nominal current (stator)	27.1 A
I_f	Field current	6.5 A
R_{ms}	Stator resistor	0.9 Ω
L_d	d-axis Inductance	4.25 mH
L_q	q-axis Inductance	12.54 mH
R_{mr}	Field winding resistor	13.8 Ω

respectively, the current waveforms of the stator and rotor of the ME are shown in figures 10, 11, and 12. The estimated and actual values of the rotor current vector modulus of the ME and the field current of the MM are shown in figures 13, 14, and 15.

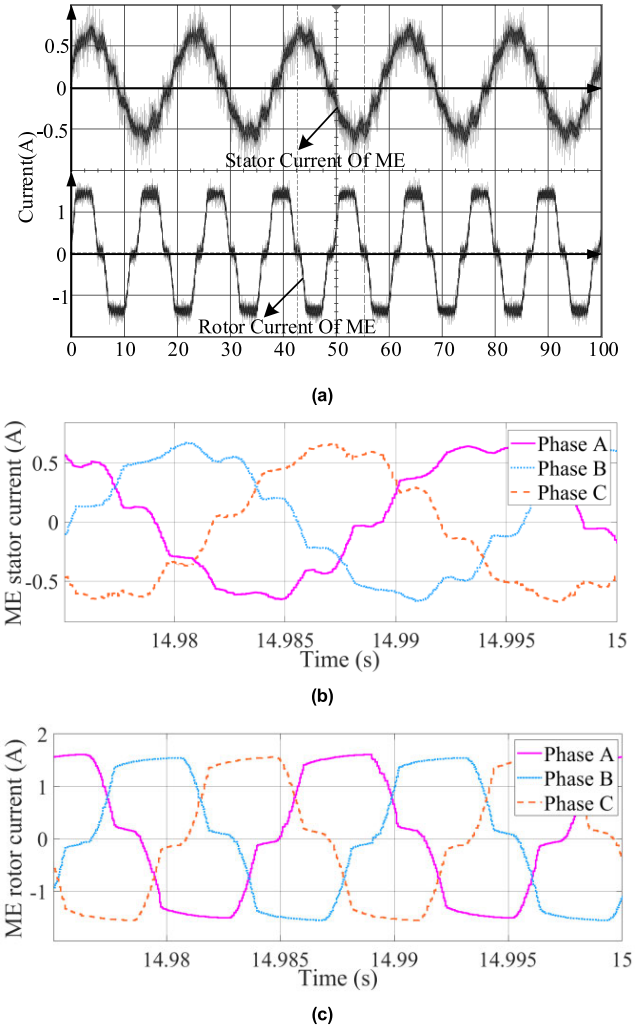

FIGURE 16. Stator and rotor current of ME at 50Hz fundamental frequency. (a) Stator and rotor current of ME measured by oscilloscope. (b) The stator three-phase current of ME measured on the experimental set. (c) The rotor three-phase current of ME measured on the experimental set.

It can be observed that the estimated value of the ME rotor current vector modulus is quite consistent with the actual value. The estimated value of MM field current is close to the actual value rather than entirely consistent, which is due to the delay, waveform distortion, and calculation deviation caused by the filter, the measurement error caused by the voltage and current sensor, and the measurement error of the system resistance inductance and other parameters. Besides, with the increases of ME source excitation frequency, the error between the estimated value and the actual value tends to increase. The reason is that the frequency of $|i_r|$ is six times of the frequency of ME stator source. And the steps running in ARM core is 20kHz, thus there are only 20Khz/(200Hz*6) =16.6 calculation steps of ME rotor CVM during a ME rotor current periods. With the decrease of calculation steps, the filter loses its efficiency, and the errors between the calculated and actual values.

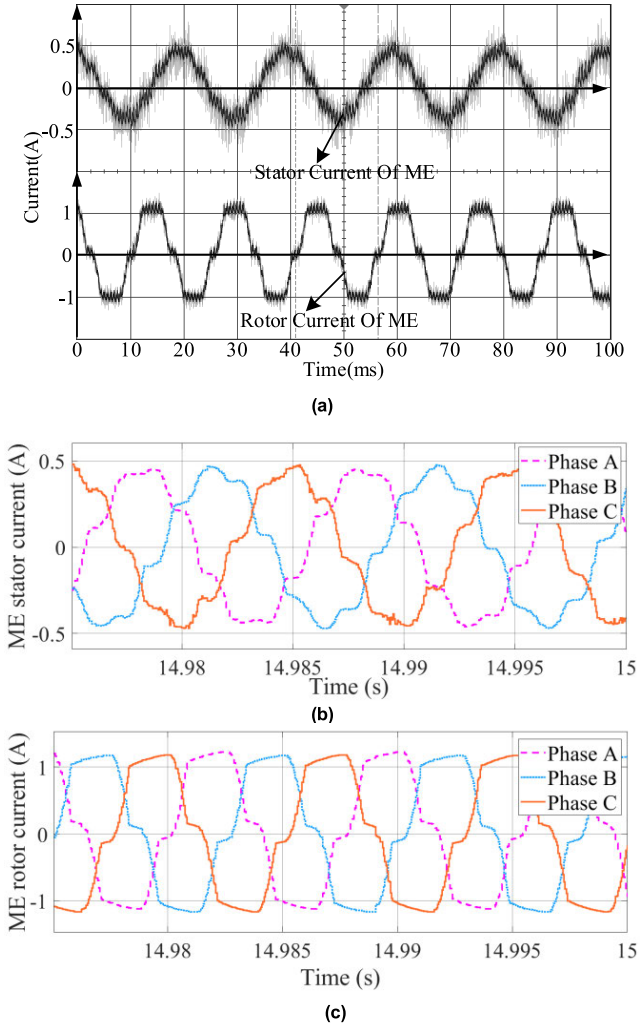

FIGURE 17. Stator and rotor current of ME at 100Hz fundamental frequency. (a) Stator and rotor current of ME measured by oscilloscope. (b) The stator three-phase current of ME measured on the experimental set.(c) The rotor three-phase current of ME measured on the experimental set.

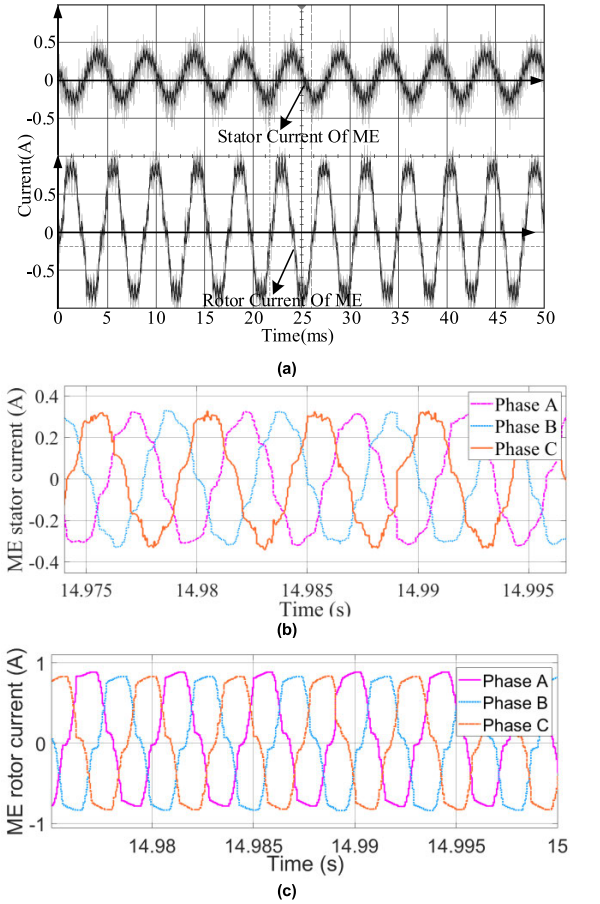

FIGURE 18. Stator and rotor current of ME at 200Hz fundamental frequency. (a) Stator and rotor current of ME measured by oscilloscope. (b) The stator three-phase current of ME measured on the experimental set. (c) The rotor three-phase current of ME measured on the experimental set.

C. ESTIMATION RESULT OF EXCITATION CURRENT WHEN MM ROTATES

When the main motor speed is 600 RPM and setting the fundamental frequency to 50Hz, 100Hz, and 200Hz, respectively, the current waveforms of the stator and rotor of the ME are shown in figures 16, 17, and 18. the estimated and actual values of the rotor current vector modulus of the ME and the field current of the MM are shown in figures 19, 20, and 21.

In the rotating state, the estimated value can be close to the actual value. However, as the fundamental frequency of the exciter excitation source increases, the error between the estimated value and the actual value shows signs of increasing. Among them, the error produced by the Max-CVM method is more significant than that produced by the Min-CVM method. There are two reasons for this phenomenon, partly caused by the estimation method's long step size. Another reason is that the high pass filtering of the voltage and current signals collected by the sensor causes the estimated CVM waveform to be slightly upturned. Since the Max-CVM

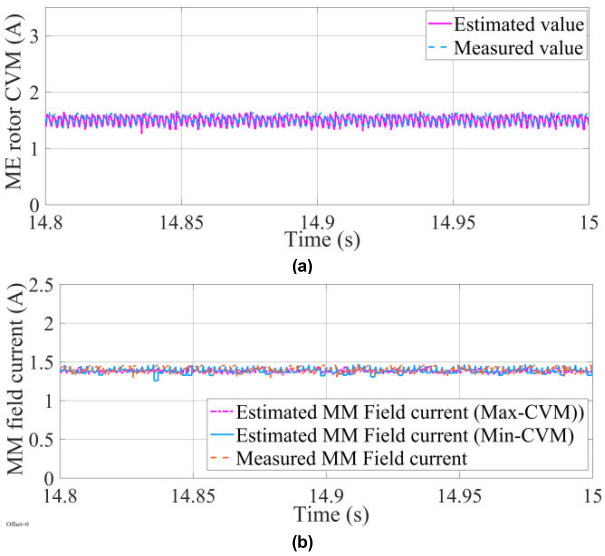

FIGURE 19. Waveform of ME rotor current and MM field current at fundamental frequency 50Hz. (a) ME rotor current Vector Modulus Waveform. (b) MM excitation current waveform.

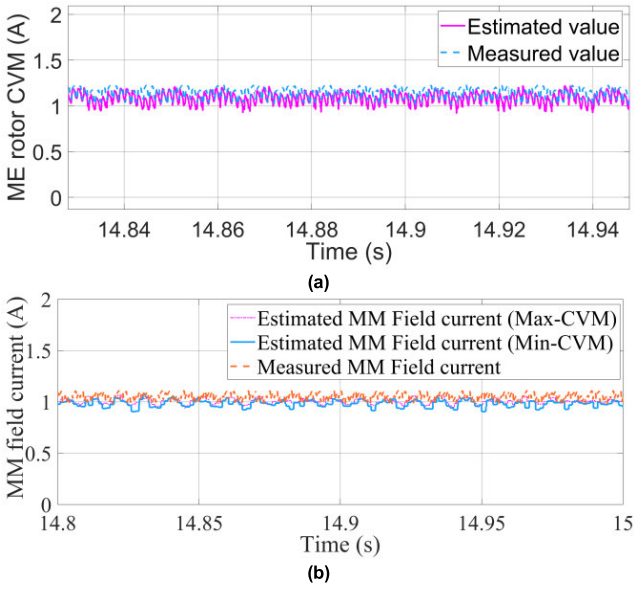

FIGURE 20. Waveform of ME rotor current and MM field current at fundamental frequency 100Hz. (a) ME rotor current Vector Modulus Waveform. (b) MM excitation current waveform.

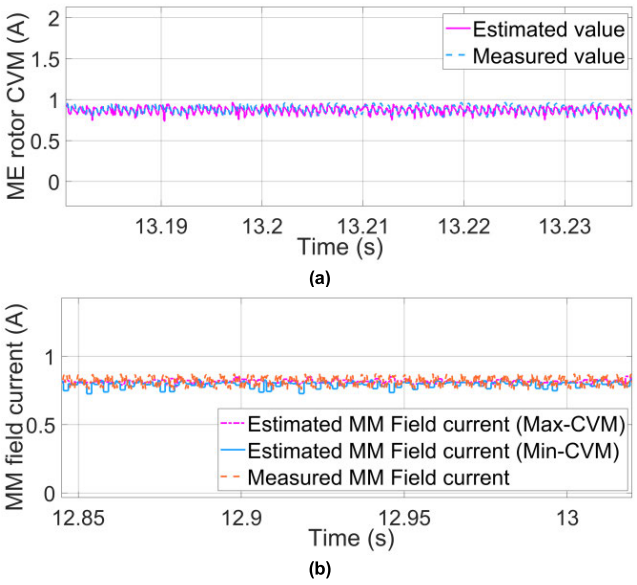

FIGURE 21. Waveform of ME rotor current and MM field current at fundamental frequency 200Hz. (a) ME rotor current Vector Modulus Waveform. (b) MM excitation current waveform.

method is based on the collection of the CVM peak value, the upturned CVM waveform causes the Max-CVM error to be larger than the Min-CVM method. Therefore, using the Min-CVM method to estimate the field current of MM is more reliable.

V. CONCLUSION

Based on the ME rotor current vector modulus, the estimating approach of the field current in the BSSG applications, is studied in this paper. It is found that the field current of MM equates to the minimum or $\sqrt{3}/2$ times maximum distance during the rotating trajectory of ME rotor CVM in a period of CVM. Thanks to the calculation of ME rotor CVM is independent of rotor position, the estimating approach of the field current becomes independent of rotor position signal too. The experiment platform is established, and the proposed method is verified experimentally in both stationary and rotating conditions.

Considering that there must be a mathematical relationship between the excitation current and the non-extremum region of CVM, suppose this relationship can be used, the process of extremum calculation can be avoided, the system delay can be reduced, and the dynamic performance of the system can be improved in the future studies.

REFERENCES

[1] B. Sarlioglu and C. T. Morris, "More electric aircraft: Review, challenges, and opportunities for commercial transport aircraft," *IEEE Trans. Transport. Electrific.*, vol. 1, no. 1, pp. 54–64, Jun. 2015.
[2] P. Wheeler and S. Bozhko, "The more electric aircraft: Technology and challenges," *IEEE Electrific. Mag.*, vol. 2, no. 4, pp. 6–12, Dec. 2014.
[3] J. Wei, Q. Zheng, M. Shi, B. Zhou, and J. Li, "The excitation control strategy of the three-stage synchronous machine in the start mode," in *Proc. IEEE Appl. Power Electron. Conf. Expo. (APEC)*, Fort Worth, TX, USA, Mar. 2014, pp. 2469–2474.
[4] J. K. Noland, S. Nuzzo, A. Tessarolo, and E. F. Alves, "Excitation system technologies for wound-field synchronous machines: Survey of solutions and evolving trends," *IEEE Access*, vol. 7, pp. 109699–109718, 2019.
[5] N. Jiao, C. Sun, X. Zhang, X. Duan, and W. Liu, "Double-side voltage-behind-reactance model of brushless exciter in aircraft wound-rotor synchronous starter-generator considering magnetic saturation," *IEEE Trans. Energy Convers.*, vol. 36, no. 3, pp. 2358–2369, Sep. 2021.
[6] Z. Zhang, W. Liu, D. Zhao, S. Mao, T. Meng, and N. Jiao, "Steady-state performance evaluations of three-phase brushless asynchronous excitation system for aircraft starter/generator," *IET Electr. Power Appl.*, vol. 10, no. 8, pp. 788–798, Sep. 2016.
[7] C. Sun, W. Liu, X. Han, X. Zhang, N. Jiao, S. Mao, R. Wang, and Y. Guan, "High-frequency voltage injection-based fault detection of a rotating rectifier for a wound-rotor synchronous starter/generator in the stationary state," *IEEE Trans. Power Electron.*, vol. 36, no. 12, pp. 13423–13433, Dec. 2021.
[8] P. C. Kjaer, T. Kjellqvist, and C. Delaloye, "Estimation of field current in vector-controlled synchronous machine variable-speed drives employing brushless asynchronous exciters," *IEEE Trans. Ind. Appl.*, vol. 41, no. 3, pp. 834–840, May 2005.
[9] N. Jiao, W. Liu, Z. Zhang, T. Meng, J. Peng, and Y. Jiang, "Field current estimation for wound-rotor synchronous starter–generator with asynchronous brushless exciters," *IEEE Trans. Energy Convers.*, vol. 32, no. 4, pp. 1554–1561, Dec. 2017.
[10] A. Griffo, D. Drury, T. Sawata, and P. H. Mellor, "Sensorless starting of a wound-field synchronous starter/generator for aerospace applications," *IEEE Trans. Ind. Electron.*, vol. 59, no. 9, pp. 3579–3587, Sep. 2012.
[11] J. Wei, H. Xu, B. Zhou, Z. Zhang, and C. Gerada, "An integrated method for three-phase AC excitation and high-frequency voltage signal injection for sensorless starting of aircraft starter/generator," *IEEE Trans. Ind. Electron.*, vol. 66, no. 7, pp. 5611–5622, Jul. 2019.
[12] J. Wei, H. Xue, B. Zhou, Z. Zhang, and T. Yang, "Rotor position estimation method for brushless synchronous machine based on second-order generated integrator in the starting mode," *IEEE Trans. Ind. Electron.*, vol. 67, no. 7, pp. 6135–6146, Jul. 2020.
[13] J. Wei, J. Wang, Z. Zhang, H. Lu, and B. Zhou, "Frequency-insensitive rotor position estimation method for three-stage synchronous machine based on indirect high-frequency signal injection," *IEEE Trans. Transport. Electrific.*, vol. 8, no. 2, pp. 1785–1793, Jun. 2022.
[14] R. Wang, W. Liu, T. Meng, N. Jiao, X. Han, C. Sun, and Y. Yang, "Rotor position estimation method of brushless electrically excited synchronous starter/generator based on multistage structure," *IEEE Trans. Power Electron.*, vol. 37, no. 1, pp. 364–376, Jan. 2022.

[15] T. Meng, W. Liu, N. Jiao, X. Han, R. Wang, and Y. Jiang, "Rotor position estimation for aviation three-stage starter/generators in the low-speed region without high-frequency signal injection," *IEEE Trans. Power Electron.*, vol. 35, no. 8, pp. 8405–8416, Aug. 2020.
[16] J. Peng, W. Liu, N. Jiao, T. Meng, Y. Zhu, and Y. Jiang, "Dual-machine injection method-based sensorless starting strategy for wound-rotor synchronous starter/generator," *IEEE Trans. Power Electron.*, vol. 34, no. 12, pp. 12310–12320, Dec. 2019.
[17] T. Meng, W. Liu, X. Han, N. Jiao, J. Peng, and Y. Jiang, "Multi-stage-structure-based rotor position estimation for a wound-field synchronous starter/generator in the low-speed region," *IEEE Trans. Power Electron.*, vol. 34, no. 12, pp. 12095–12105, Dec. 2019.
[18] S. Mao, W. Liu, Z. Chen, N. Jiao, and J. Peng, "Rotor position estimation of brushless synchronous starter/generators by using the main exciter as a position sensor," *IEEE Trans. Power Electron.*, vol. 35, no. 1, pp. 800–815, Jan. 2020.
[19] S. Mao, W. Liu, N. Jiao, F. Gao, and Z. Chen, "Sensorless starting control of brushless synchronous starter/generators for the full-speed range," *IEEE Trans. Power Electron.*, vol. 35, no. 8, pp. 8347–8360, Aug. 2020.
[20] Z. Zhang, W. Liu, J. Peng, D. Zhao, T. Meng, J. Pang, and C. Sun, "Identification of TBAES rotating diode failure," *IET Electr. Power Appl.*, vol. 11, no. 2, pp. 260–271, Feb. 2017.
[21] J. Pang, W. Liu, Z. Wei, C. Sun, N. Jiao, and X. Han, "Online diode fault detection in rotating rectifier of the brushless synchronous starter generator," *IEEE Trans. Ind. Informat.*, vol. 16, no. 11, pp. 6943–6951, Nov. 2020.

ZAN ZHANG was born in Xuchang, Henan, China, in 1984. He received the M.S. degree in electrical engineering from Henan Polytechnic University, Jiaozuo, China, in 2012, and the Ph.D. degree in electrical engineering from Northwestern Polytechnical University, Xian, China, in 2018.

Then, he worked with Xuchang University, Xuchang. His research interests include aircraft starter/generator, and design, analysis, and control of PMSMs.

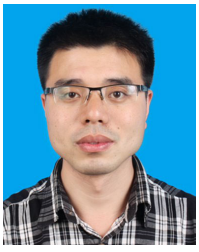

WEIZHOU LI was born in Neihuang County, Hennan, China, in 1988. He received the B.S. degree in electrical engineering from Xuchang University, and the M.S. degree in power electronics and electric drives from the Hunan University of Technology, in 2014.

From 2014 to 2019, he was a Teaching Assistant with the Engineering Technology Training Center, Xuchang University, and has been a Lecturer, since 2020. His current research interests include the area of electric machines and drives.

LUHUAN SHI was born in Luoyang, Henan, China, in 1984. She received the master's degree in electrical engineering from the Changchun University of Technology, Changchun, China, in 2009. She joined Xuchang University, in 2009, as a Lecturer. She has been at the School of Electrical and Mechanical Engineering. She has authored or coauthored over ten journal articles and conference papers, in 2013. She holds 11 patents. Her current research interests include complex system simulation and electrical control.

JUNLEI MA was born in Xuchang, Henan, China, in 1983. He received the B.S. degree in automation and the M.S. degree in detection technology and automation from Zhengzhou University, Zhengzhou, China, in 2005 and 2008, respectively.

From 2016 to 2019, he was a Research Assistant with the Engineering Training Center, Xuchang University, where he has been a Lecturer with the Engineering Training Center, since 2020. His research interests include motion control systems, intelligent robots, and artificial intelligence.

ZHIFENG YIN was born in Xuchang, Henan, China, in 1975. He received the M.S. degree from Lanzhou University, Lanzhou, China, in 2012.

Then, he worked with Xuchang University (XCU), Xuchang, where he is currently a Professor with the School of Electrical and Mechanical Engineering. He is also the Dean of Electrical and Mechanical Engineering. His research interests include aircraft starter/generator, and design, analysis, and control of PMSMs.